Pergamon

Journal of Structural Geology, Vol. 19, No. 12, pp. 1479 to 1493, 1997

PII: S0191-8141(97)00075-8
0191-8141/97 $17.00 + 0.00

Geometric analysis and scaling relations of deformation bands in porous sandstone

HAAKON FOSSEN

Department of Geology, University of Bergen, Allégt. 41, N-5007 Bergen, Norway

and

JONNY HESTHAMMER

Statoil, GF/PETEK-GEO, N-5020 Bergen, Norway

(*Received* 24 *February* 1997; *accepted in revised form* 12 *September* 1997)

Abstract—Displacement, length and linkage of deformation bands have been studied in Jurassic sandstones in southeastern Utah. Isolated deformation bands with lengths (L) that span more than three orders of magnitude show similar displacement (D) profiles with more or less centrally located maxima and gently increasing gradient toward the tips. Soft- and hard-linked examples exhibit steeper displacement gradients near overlap zones and immature hard links, similar to previously described fault populations. The deformation band population shows power-law length and displacement distributions, but with lower exponents than commonly observed for populations of larger faults or small faults with distinct slip surfaces. Similarly, the D_{max}–L relationship of the deformation bands shows a well-defined exponent of *ca* 0.5, whereas the general disagreement for other fault populations is whether the exponent is 1 or 1.5. We suggest that this important difference in scaling law between deformation bands and other faults has to do with the lack of well-developed slip surfaces in deformation bands.

During growth, deformation bands link to form zones of densely spaced bands, and a slip surface is eventually formed (when 100 m $< L <$ 1 km). The growth and scaling relationship for the resulting populations of faults (slip surfaces) is expected to be similar to 'ordinary' fault populations. A change in the D_{max}–L scaling relationship at the point when zones of deformation bands develop slip surfaces is expected to be a general feature in porous sandstones where faults with slip surfaces develop from deformation bands. Down-scaling of ordinary fault populations into the size domain of deformation bands in porous sandstones is therefore potentially dangerous.

INTRODUCTION

There has been a rapidly growing interest in fault geometry and the distribution of fault attributes such as length, surface area, thickness and displacement in faulted rocks during the last decade. Of particular interest are scaling laws for fault populations, fault-growth models and complicating factors, such as fault linkage during growth. Data have been collected in various ways, for example from satellite images, aerial photographs, seismic data and regular outcrop studies. The total database is still quite small, mostly due to the difficulty in extracting high-quality fault geometry data from naturally deformed rocks. This has contributed to a general controversy over fault scaling exponents. However, not only is expansion of the existing global database necessary to explore this disagreement, but also consistent sets of data, collected from single lithologies with a common and simple tectonic history (e.g. Scholz *et al.*, 1993).

In this article we present fault geometry data from deformation bands (e.g. Antonellini *et al.*, 1994; also known as granulation seams, microfaults or shear bands) in the San Rafael Desert, Utah, U.S.A. The dataset spans more than three orders of magnitude for fault length (0.05–100 m) and more than two orders of magnitude for displacement (0.2–33 mm), and thus provides an important set of data to the study of scaling relationships.

GEOLOGICAL SETTING AND GENERAL DESCRIPTION

The study area is located near Wildhorse Spring, about 2 km north of Goblin Valley State Park and Wild Horse Butte in southeastern Utah, U.S.A. Exposed surfaces of the Jurassic Entrada Formation (see Rigby, 1987, and references therein for stratigraphic descriptions) are exposed along the eastern side of the road, just north of a short dirt road to Wild Horse Creek (Fig. 1). The lower part of the Entrada Formation was studied, which here consists of a *ca* 20 m thick dark red sandstone overlain by grey (3–4 m), red (3–5 m) and pale yellow (6–10 m) sandstones. The sandstones consist mainly of quartz and feldspar, and are very porous (porosity of *ca* 25%). The data presented below were collected from the pale yellow sandstone.

Structurally, the Goblin Valley area is located on the down-thrown southeastern margin of the San Rafael Swell (Rigby, 1987), where the Mesozoic strata have retained a subhorizontal orientation. Fault structures in the study area are part of a regional system of ESE–

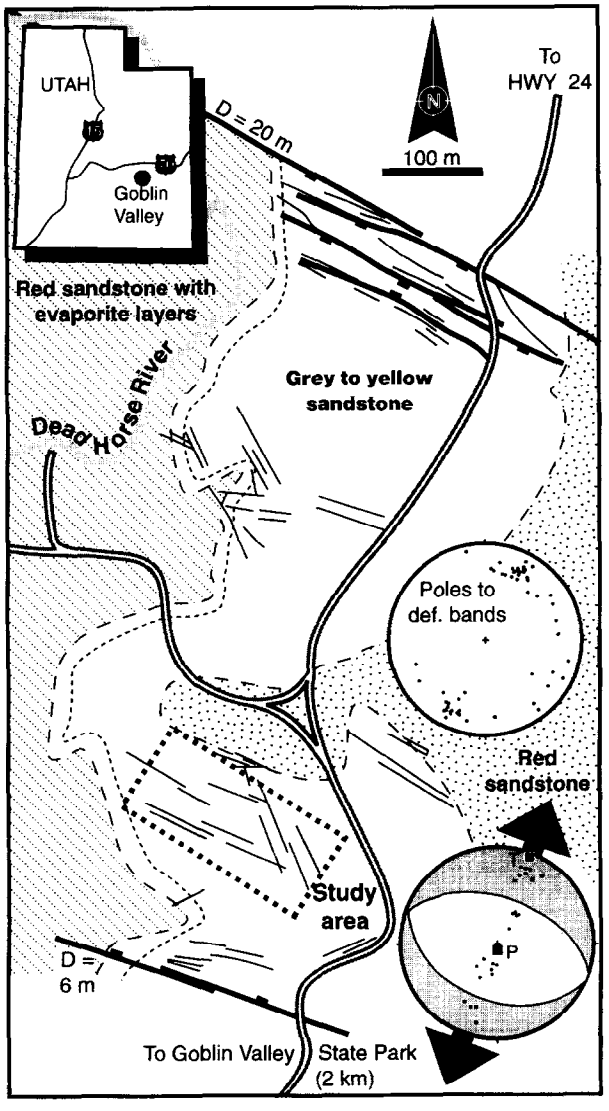

Fig. 1. Geological map of the study area in southeastern Utah. Thin lines indicate deformation band systems, while thick lines mark deformation band cluster zones with associated slip surfaces (faults). The sandstones belong to the Entrada Formation. The upper equal-area plot shows the orientation of measured deformation bands, while the lower plot indicates the extension direction from kinematic analysis of slip surfaces as outlined by Marrett and Allmendinger (1990). The broken line outlines the study area where deformation bands were measured.

WNW-trending faults that run across the San Rafael Swell (Baker, 1946). This fault system has been described from the Molly's Castle area some 2 km southeast of the present study area (Aydin, 1978; Aydin and Johnson, 1978, 1983; Aydin and Reches, 1982).

The area studied is part of a small (600–700 m wide) graben structure, bounded by two ESE–WNW-striking faults, each of which has up to 20 m displacement. Kinematic analysis of striated surfaces of these faults indicate NNE–SSW extension and vertical shortening (Fig. 1). The graben area contains abundant minor structures (deformation bands), of which the majority are subparallel to the main faults (WNW–ESE), some are NNW–SSE trending, and some show different orientations (Fig. 1).

Deformation bands

Deformation bands occur in porous sandstones in many parts of the World (Pittman, 1981; Jamison, 1982; Underhill and Woodcock, 1987; Fowles and Burley, 1994), and have been described in much detail from the Entrada and Navajo sandstones of southeastern Utah (Aydin, 1978; Aydin and Johnson, 1978, 1983; Antonellini and Aydin, 1994, 1995; Antonellini *et al.*, 1994). In this area three kinds of deformation bands are distinguished (Antonellini *et al.*, 1994): (1) deformation bands with little or no cataclasis; (2) deformation bands with cataclasis; and (3) deformation bands with clay smearing. We are concerned with the second type, which are thin (mm-thick) brittle shear zones (Ramsay, 1980) dominated by cataclastic processes, and typically with a few millimetres or centimetres of displacement (Fig. 2a–c). As will be discussed below, they have geometries that are similar, but not necessarily identical, to those of larger faults. Furthermore, they tend to develop into narrow zones consisting of several intricately associated and interconnected deformation bands, in which a slip plane eventually forms to accommodate further displacement along the zone (Aydin and Johnson, 1978, 1983).

Deformation bands in the Goblin Valley area generally involve cataclastic deformation which dramatically reduces grain size, porosity and permeability within the bands. Reductions in permeability within this type of deformation band is estimated to be up to three orders of magnitude (Gabrielsen and Koestler, 1987; Antonellini and Aydin, 1994), proving their significance as barriers to fluid flow in a reservoir setting. Systematic sectioning indicates that the deformation bands in the Goblin Valley area are approximately dip-slip structures with normal-sense movements, and linear corrugations on some of the nicely weathered-out deformation bands (Fig. 2) support this interpretation (see below). In vertical sections, oppositely dipping deformation bands show mutual cross-cutting relationships typical for contemporaneous movement as described by Horsfield (1980).

DATA COLLECTION METHOD

The Entrada sandstone is poorly consolidated so that small holes can be made along each deformation band with a hammer and chisel (Fig. 2a). Steeply dipping cuts were made perpendicular to the deformation bands where laminations were seen. By wetting these cuts, the lamination and its apparent offset across the deformation band could be seen more clearly, and the vertical offset (throw) was measured. As argued above, the deformation bands are generally dip-slip structures and the apparent offset observed in any of the vertical sections is in all cases assumed to approximate the maximum displacement. Because the deformation bands are steeply dipping (*ca* 70°), the throw and displacement are almost identical (within 7% error). The uncertainty involved during

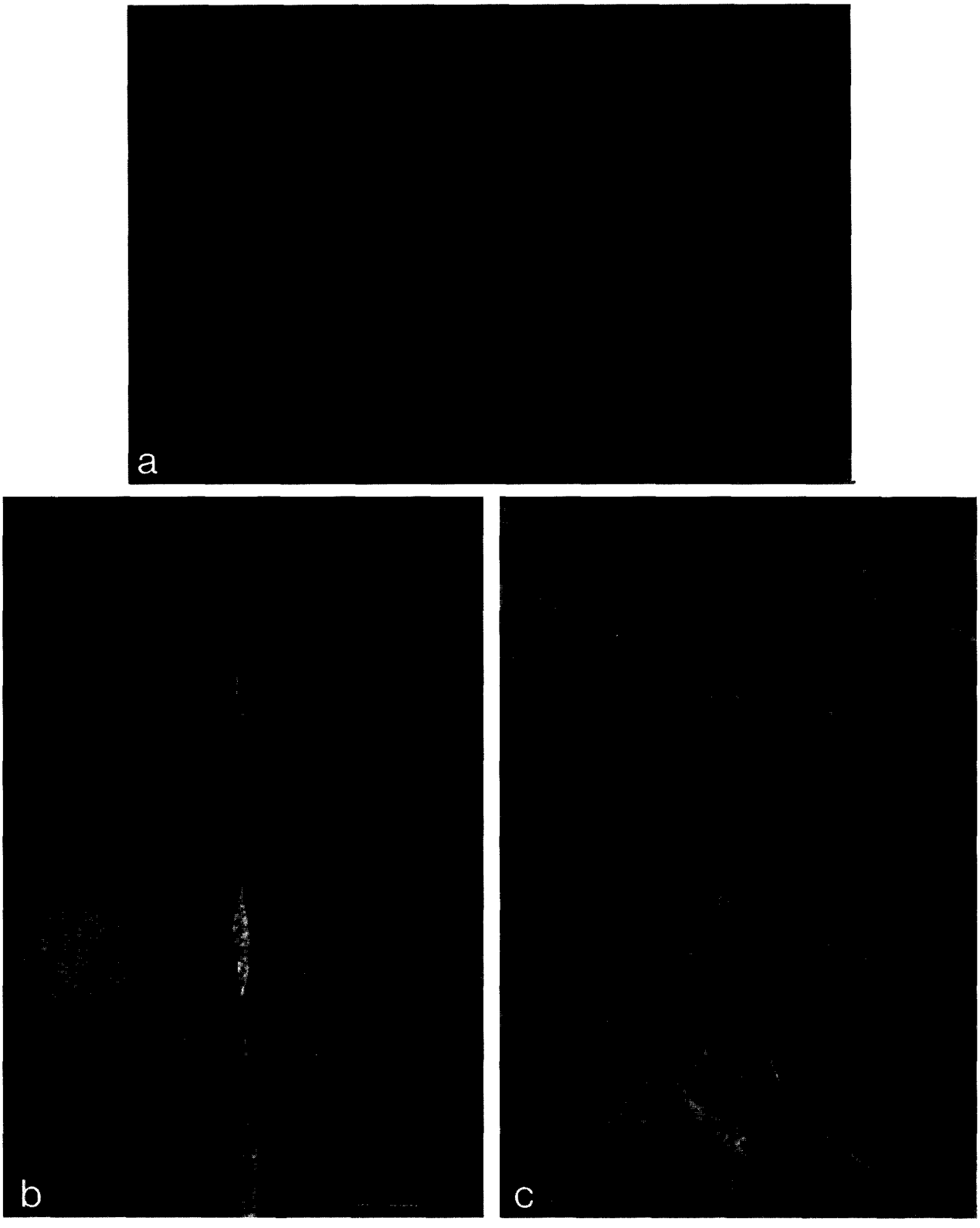

Fig. 2. (a) Single, steeply-dipping deformation band in the Entrada Formation. (b) Lens-shaped clusters of deformation bands at the cm-scale. (c) Hard-linked system of deformation bands. The links have a consistent left-stepping geometry.

measurement depends on the quality of the cut, i.e. the sharpness of laminae as they appeared in the sections, and the amount of time spent to find the best sections through the structures. An effort was made to obtain measurements with errors no larger than ± 0.5 mm for small ($D < 5$ mm) deformation bands, which were examined very carefully, and ± 1 mm for larger ones.

A total of 50 deformation bands, or systems of deformation bands, were examined using the above-mentioned method. Thirty-one of these were considered

to be isolated structures. In addition, 10 soft-linked systems (terminology of Walsh and Watterson, 1991) that consisted of a total of 23 segments, and nine systems of hard-linked deformation bands (a total of 25 segments) were mapped.

OBSERVATIONS

On the surfaces studied the deformation bands occur as: (a) isolated structures; (b) relatively simple systems of linked deformation bands; and (c) dense cluster zones with associated slip surface(s) (Figs 2 & 3).

Isolated deformation bands

Isolated deformation bands are defined here as those that do not interfere with other deformation bands in map view, and where their tip points are more than *ca* 40 cm away from its nearest neighbour (most are considerably further away than 40 cm). The exception to this rule is where the 'isolated' deformation band cuts, or is cut by, another deformation band which, from offset relationships, is older or younger in age. Where the distance between the tips is closer than *ca* 40 cm, the segments typically appear to be part of a multisegmented soft-linked system, as seen by the curving of overlapping tips, an unusual rapid decrease in displacement towards the tip points, etc. (see below). The isolated deformation bands may or may not interfere with other bands in the vertical dimension, of which we have no control. In general, the longer the deformation band, the more likely it is to interfere with another band and form a linked system. Hence, there is an abundance of short, isolated deformation bands in the area.

Whereas single deformation bands typically have thicknesses of *ca* 1 mm, they may locally widen along strike to form lenses *ca* 1 cm wide and a few centimetres long, as shown in Fig. 2(b). Such lenses may represent early small-scale bridge structures between what were individual deformation band segments at an early stage. No displacement anomalies are associated with these lenses, and deformation bands with such structures are therefore included in the isolated deformation band population in this study.

Displacement profiles for isolated or approximately isolated deformation bands are shown in Fig. 4, where they are arranged according to their length (increasing

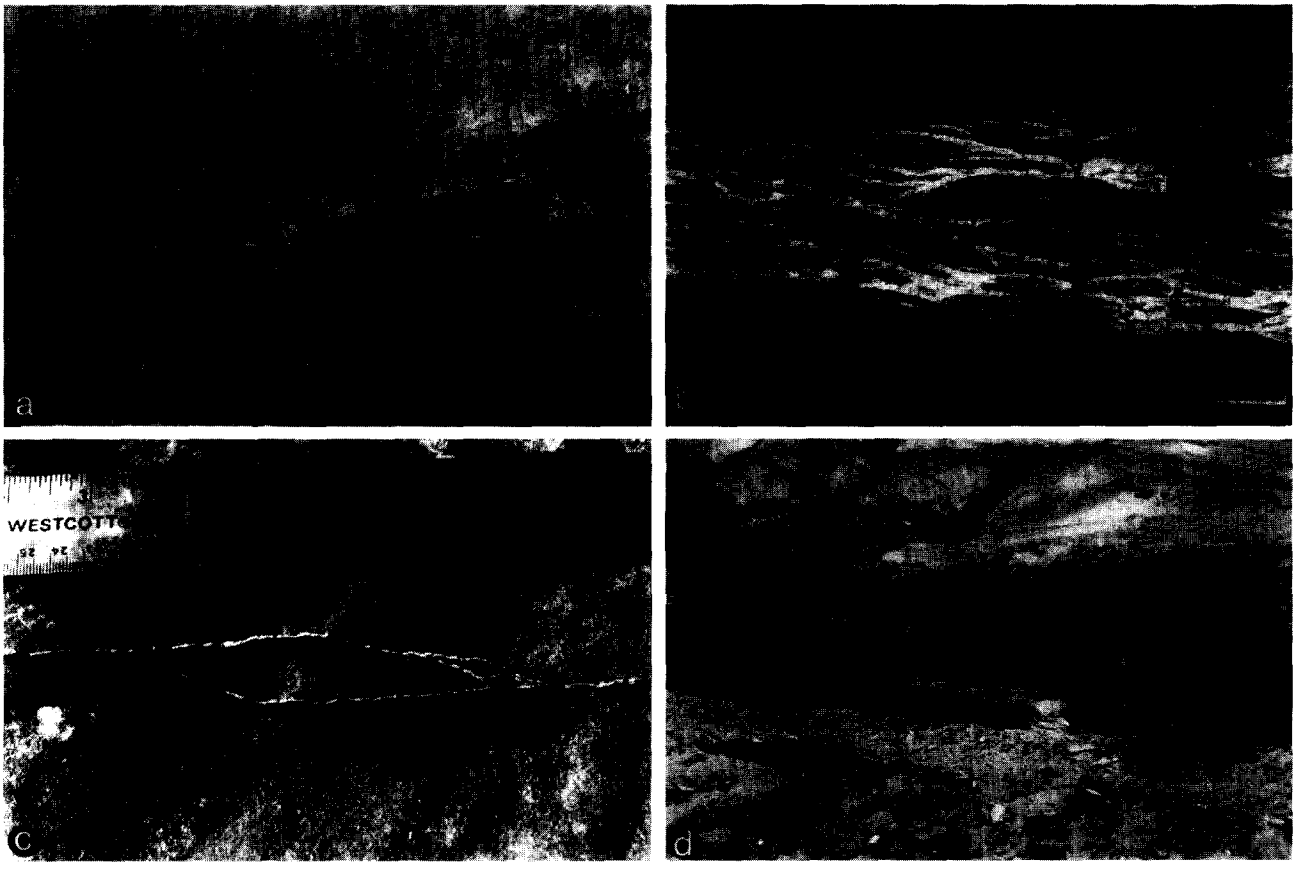

Fig. 3. (a) Hard-link between deformation band segments, where one segment curves and joins with a straight segment. Numbers indicate displacement (in mm), which rapidly changes across the intersection for the straight segment. (b) Deformation band cluster zone, as seen in the horizontal section. Note the anastomosing deformation bands (light-coloured). (c) Hard-link where both deformation bands curve and join, indicating contemporaneous development. (d) Corrugations developed along margins of the cluster zone (b) above, consistent with dip-slip movement.

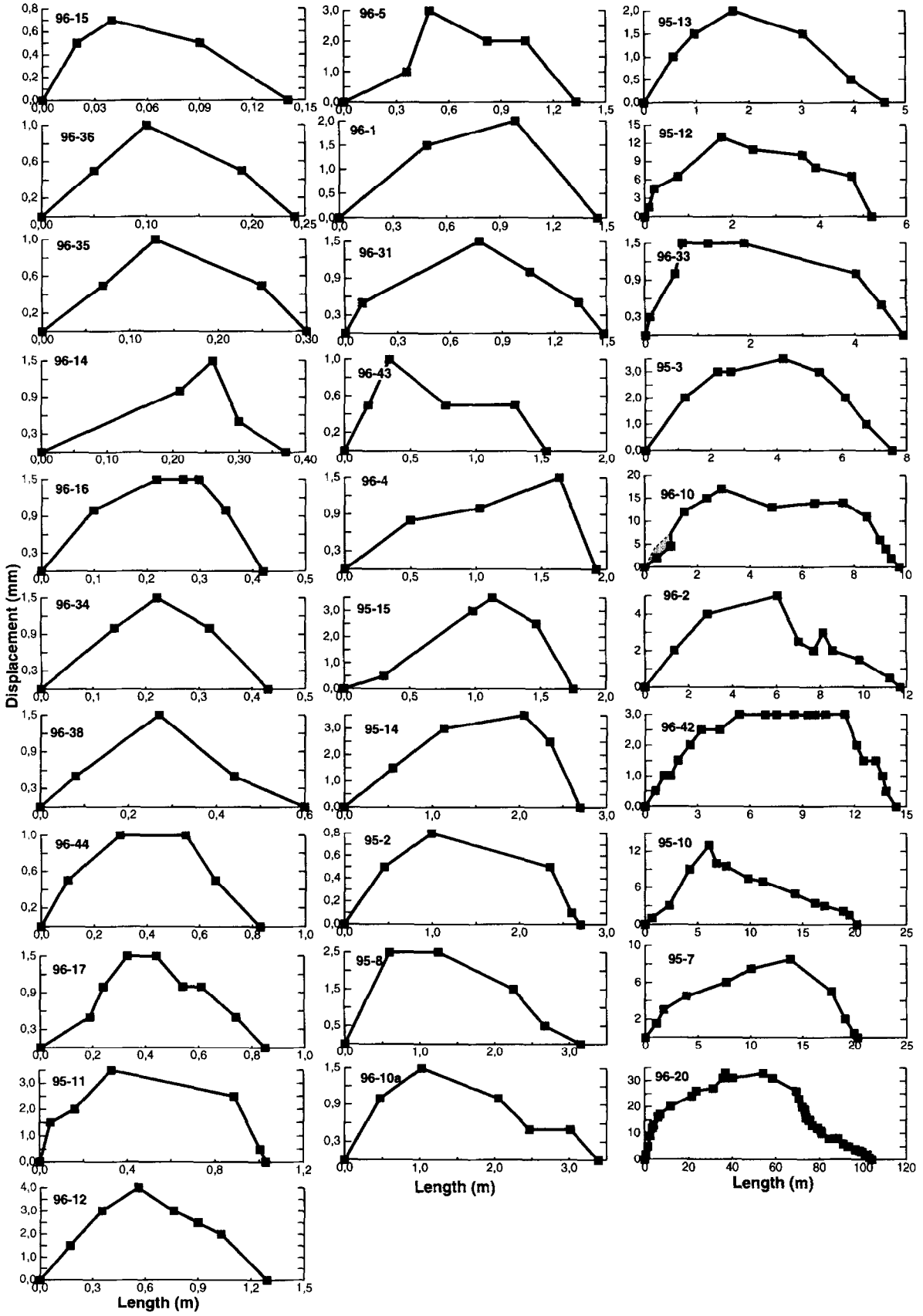

Fig. 4. Displacement profiles for isolated deformation bands, arranged according to length (increasing downwards in the figure). Horizontal scale in metres, vertical scale in millimetres.

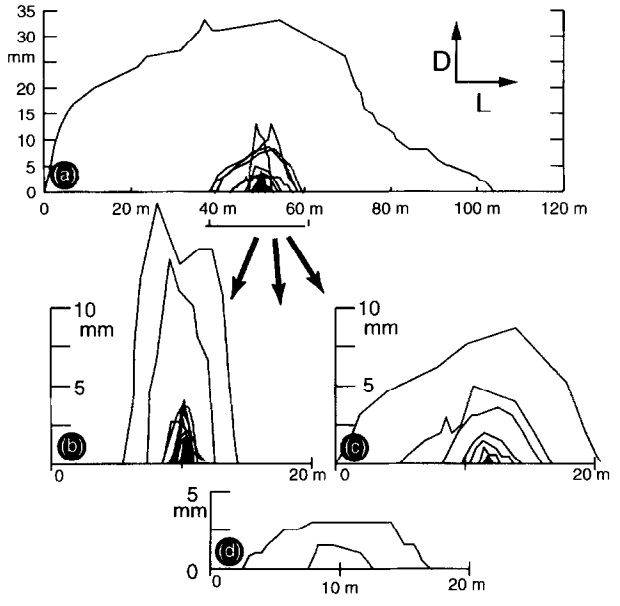

Fig. 5. (a) Isolated deformation bands plotted in a single diagram. (b)–(d) A selection of deformation bands grouped based on their geometric similarities. The categories are here termed peak (b), intermediate (c) and plateau type (d).

length downward and to the right in the figure). No obvious difference in displacement profile is seen between short and long deformation bands. The displacement maximum may be located in the central portion of the bands, although in many cases the maximum is clearly off-centre. Most of the displacement profiles show a clearly defined peak, and only a few (e.g. 96-42) show a central plateau of more or less constant displacement.

In Fig. 5(a) the displacement profiles are plotted together, centred at the same point along the x-axis. The different shapes of the profiles are more clearly displayed in this figure. In order to illustrate the variation in profile geometries, the displacement profiles have been subdivided into three categories in Fig. 5: peak type (Fig. 5b); intermediate (Fig. 5c); and plateau-type profiles (Fig. 5d).

The largest isolated deformation band in Fig. 5(a) is not included in Fig. 5(b–d), but can be seen to be of the intermediate type. Plateau-type profiles are very uncommon among isolated deformation bands, and none are observed among the many short (< 5 m long) structures measured. Plateau-type profiles are characteristic of linked systems, as described below. Because the profiles were sampled along arbitrary sections through deformation band surfaces, most of them are off-centre, i.e. they do not cross close to the point of maximum displacement on the surface. Qualitatively this should result in more plateau-like profiles (Muraoka and Kamata, 1983; Walsh and Watterson, 1988), and it may be speculated that the peak-type profiles sample the central and intermediate part of the deformation band surface, whereas profiles with less well-developed peaks represent more marginal sections.

In the model of Cowie and Scholz (1992), the shape of the displacement profile and the ratio of maximum displacement (D_{max}) to length (L) are a function of the shear strength of the rock. The Cowie and Scholz (1992) model predicts that faults in different tectonic regions and rock types will have a different D_{max}/L ratios. In particular, they suggest a distinction between faults that cut the entire thickness of the brittle upper crust and those that do not. In our example, faults are small enough that layering may play a similar role, i.e. the shape of the D–L profile may depend on whether the faults are confined to a certain layer or not, and on the physical properties of the layer(s). However, extreme lithological contrasts, such as those described from Flamborough Head by Peacock and Sanderson (1994) and Nicol *et al.* (1996), are not apparent in the present study area at the scale of observation.

To compare the gradients in all the isolated deformation bands, the normalized lengths from the tips to the point of maximum displacement are plotted against normalized displacement (D/D_{max}) for each of the isolated deformation bands in Fig. 6(a & b). The plots indicate that some deformation bands have a sublinear increase in displacement towards their maxima, while the majority have higher gradients near the tips that gradually decrease towards their central area. This is illustrated by the second-degree polynomial function that has been fitted to the dataset in Fig. 6(a). The very steep gradient near isolated fault tips predicted by linear elastic theory (discontinuous line or half-ellipse in Fig. 6; e.g. Pollard and Segall, 1987) is not seen. Similarly, the tapered or bell-shaped displacement profile predicted by the Cowie and Scholz (1992) model is not reflected in the present data, indicating that deformation bands deviate from these simple models.

Soft-linked systems

Some of the deformation bands occur as subparallel, en échelon arranged structures with overlapping tips. Where the distance separating the deformation band traces is approximately an order of magnitude less than the individual deformation band lengths, the constituents may be regarded as a soft-linked (e.g. Walsh and Watterson, 1991) system of deformation bands. The different types of links that are observed in the study area are shown schematically in Fig. 7.

Some well-exposed examples of soft-linked systems were mapped in detail, and their geometries and displacement profiles are shown in Fig. 8. Many of the overlaps are characterized by perfectly parallel and straight segments (95-6/7, 95-11/12, 95-14/15, 96-6 and 96-7), whereas in other cases one or both of the tips are curved (e.g. 96-11; see Fig. 7b–c). In the latter case, the resulting structure is known as an open eye-structure. Eye-structures have been interpreted as being formed where the local crack-induced stresses dominate over remote stresses (Olson and Pollard, 1989; Cruikshank *et al.*, 1991). Parallel overlapping tips, however, imply the dominance of a remote compressive crack-parallel differ-

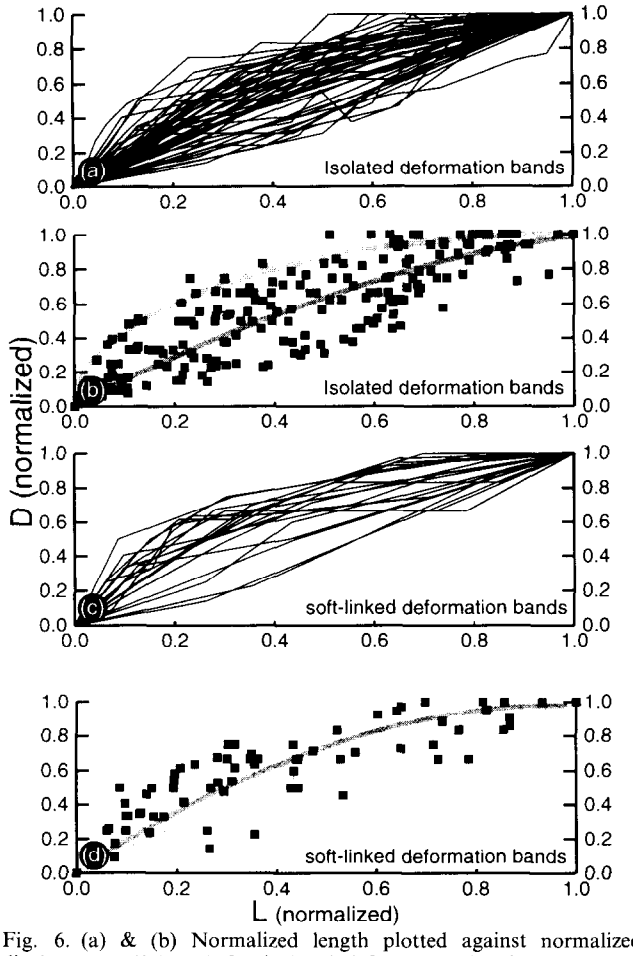

Fig. 6. (a) & (b) Normalized length plotted against normalized displacement (D/D_{max}) for isolated deformation bands. The length here is the normalized distance from one of the tip points to the point of maximum displacement. Each fully measured deformation band therefore gives rise to two curves or two sets of data points. Data from isolated halves of soft-linked systems are included. The upper, broken line in (b) indicates the profile predicted by linear elastic theory (e.g. Willemse *et al.*, 1996), while the lower solid line represents the best-fit third-order polynomial fit to the data. (c) & (d) Same as (a) & (b), but for soft-linked half-segments. A steeper gradient in the tip area is recognized for (c) & (d). The solid line in (d) represents the best-fit third-order polynomial fit to the data, and the dashed line indicates the best-fit polynomial in (b) (for comparison).

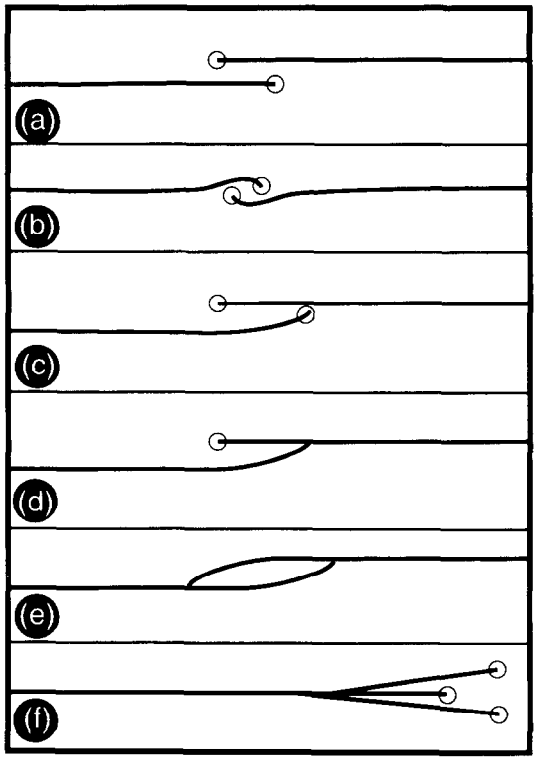

Fig. 7. The different types of overlap or tip interaction observed in the study area. (a)–(c) are soft linked, while (d) & (e) show hard-linked structures. The small circles indicate free tip-points.

ential stress (Olson and Pollard, 1989). The coexistence of both types of structures along systems of apparently coeval deformation bands may indicate that the local stress conditions changed rapidly during deformation or, more likely, that propagation of deformation bands may not be analogous to the idealized crack propagation modelled by Olson and Pollard (1989).

In Fig. 8, the systems are arranged according to degree of overlap. The uppermost system (96-32) consists of two deformation band segments where there is no overlap or underlap. In this case the left-hand segment of the system shows very small displacement changes in its central part (plateau-type), which perhaps is related to its nature as a hard-linked system at smaller scale (see below). In cases like this, where deformation band segments do not overlap or underlap, the combined displacement curve reaches zero at the minimum between the peaks. With increasing degree of overlap (downward in Fig. 8), the minimum of the summed displacement curve becomes less marked (for example, see system 96-30 in Fig. 8). In the lowermost example of Fig. 8 (system 96-7), three segments overlap to the extent that the combined displacement profile mimics that of a single deformation band of similar total length, or a hard-linked system of the kind shown as system 96-3 in Fig. 9.

From Fig. 8 it is reasonable to assume that soft-linked systems of deformation bands in the study area developed as geometrically non-coherent individual segments until the degree of overlap resulted in a combined system that continued to be geometrically coherent (i.e. their combined displacement profile resembles that of an isolated fault). During this process, which is illustrated schematically in Fig. 10, we believe that the system develops from the non-coherent multipeak-type profile (a & b) through a plateau-type profile (c) to a coherent single-peak profile (d) (see also Childs *et al.*, 1995; Dawers and Anders, 1995).

For the majority of the deformation bands, the gradient is steeper towards the tip in the overlap zone than towards the independent tip. This general trend is confirmed by plotting normalized displacement against normalized distance from the tips in the overlap zones towards the displacement maxima (Fig. 11), and confirms theoretical modelling and observations of natural fault populations (e.g. Peacock and Sanderson, 1991; Trudgill and Cartwright, 1994; Dawers and Anders, 1995; Huggins *et al.*, 1995; Willemse *et al.*, 1996).

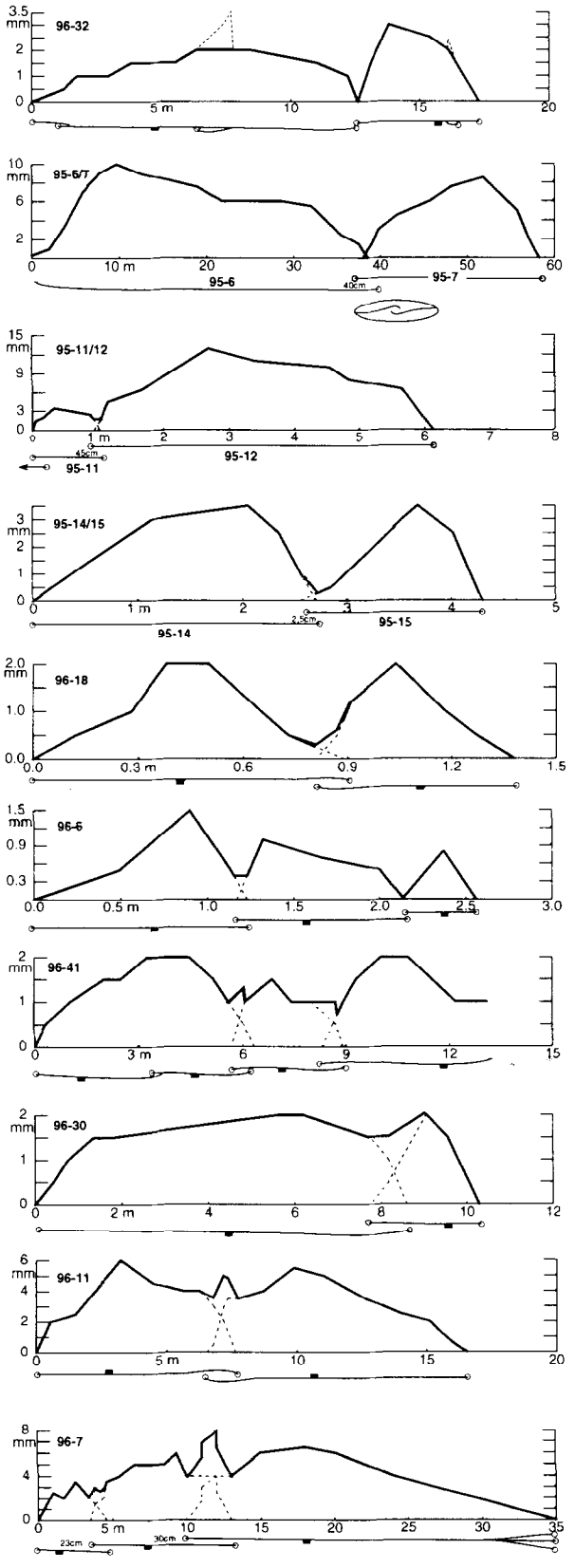

Fig. 8. Displacement profiles of soft-linked systems of deformation bands measured in the field. Arranged according to an increasing degree of overlap (downwards in the figure). Map sketches below each graph indicate the geometry of the systems. The bar indicates the downthrown side. The stipled peak in the upper diagram indicates the displacement contribution from the minor branch indicated in the sketch map below the graph.

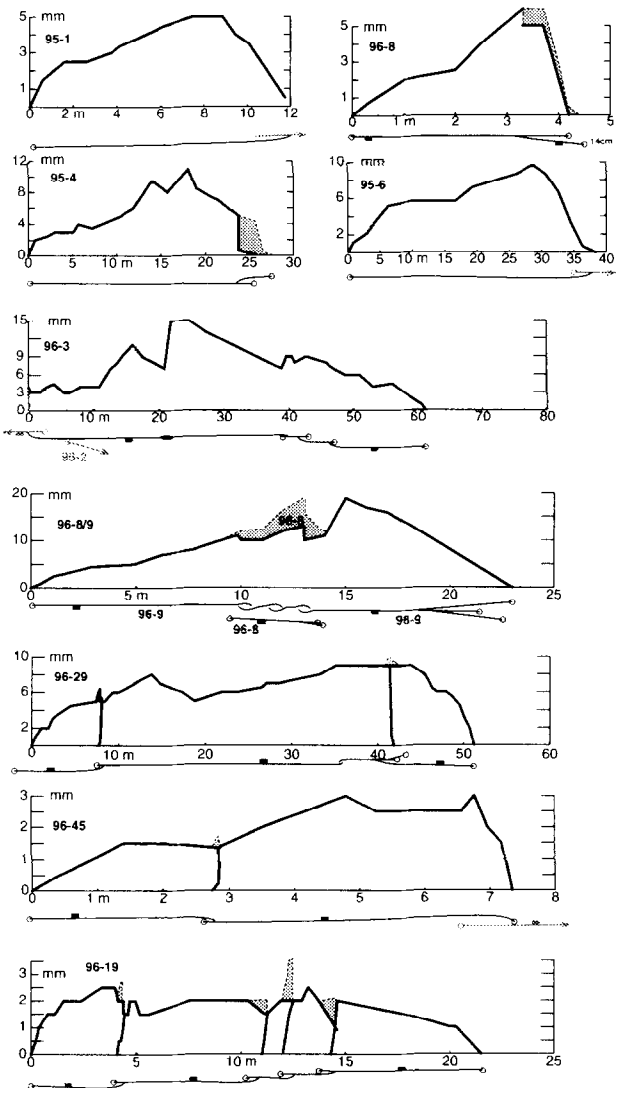

Fig. 9. Displacement profiles of hard-linked systems of deformation bands measured in the field. Shaded areas indicate the displacement contributions from minor branches indicated in the sketch maps below each graph. See text for discussion.

Hard-linked systems

In contrast to soft-linked systems of deformation bands, hard-linked systems (also called breached overlap zones; Childs *et al.*, 1995) occur where individual segments have physically joined in the section studied, and therefore can be traced continuously from one end of the system to the other.

The most frequently observed hard link is where a straight segment veers and joins with a parallel, neighbouring straight segment, and where the latter terminates soon after the point of intersection (Figs 3a & 7d). Two of the examples from Fig. 9 (95-1 and 95-6) and an additional example in Fig. 8 (95-6, left part) exhibit displacement profiles with a steep gradient along the *curving* segment of the link. The curving tips are linked with *straight* segments which show a much more extreme decrease in displacement from the link to its point of

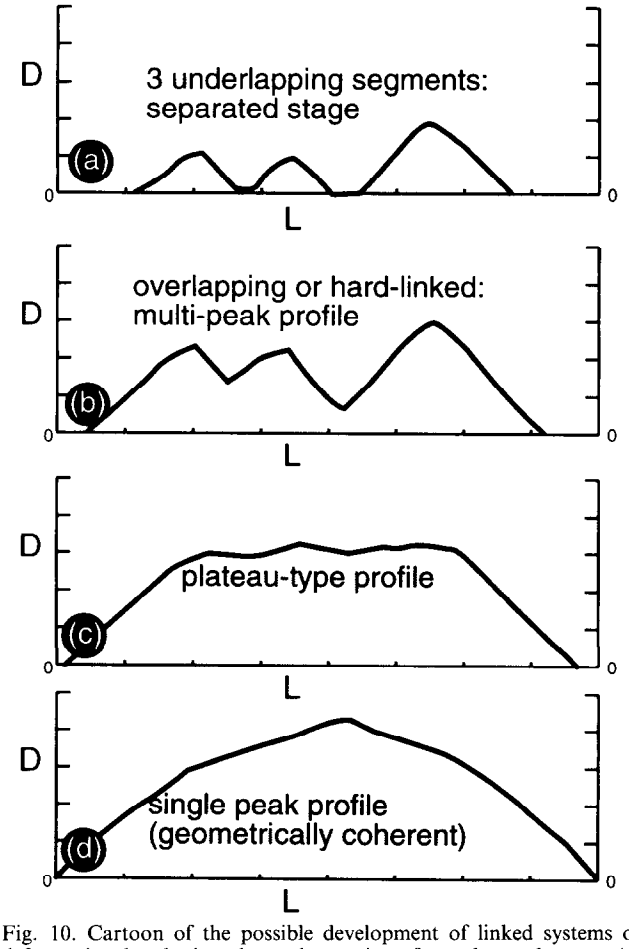

Fig. 10. Cartoon of the possible development of linked systems of deformation bands, based on observations from the study area. (a) Three underlapping deformation bands grow individually and the tips are approaching each other. (b) Tips overlap (link softly) or connect, and a combined multipeak displacement profile results. (c) If the system does not run into and incorporate new deformation bands, a flat, plateau-type profile is formed, which gradually transforms into a single peak displacement profile akin to that of a single, isolated deformation band.

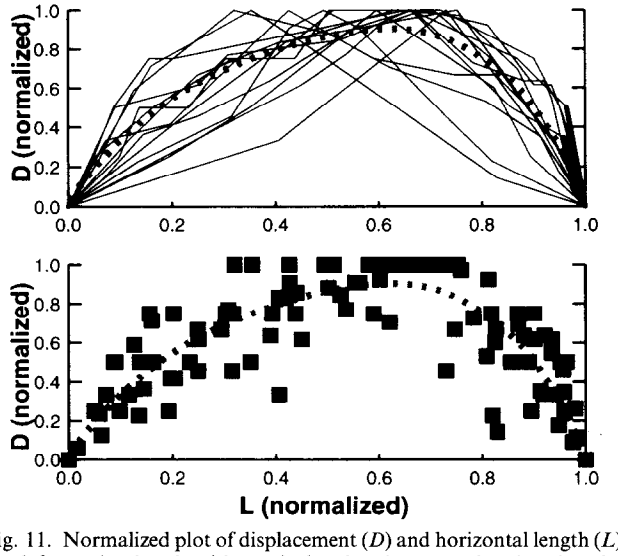

Fig. 11. Normalized plot of displacement (D) and horizontal length (L) for deformation bands with one isolated and one overlapping tip. The length is measured from the isolated tip. The best-fit second-order polynomial is shown. Note the skewness of the distribution. See text for discussion.

termination (e.g. Fig. 3a and lower three systems in Fig. 9). In other words, the straight segments do not extend far beyond their points of linkage, as displacement is efficiently transferred to the curving connecting segment.

When observed in joint systems, the type of hard link discussed above (Fig. 7d) has been interpreted to indicate a relative age difference between the linking segments (Cruikshank and Aydin, 1995). The straight segment is considered to be older, and the curved one veers as it approaches and becomes influenced by the local variation in stress field caused by the already existing straight segment. At early stages after linking, a decrease in displacement along the curving segment occurs because of the locking effect prior to hard-linking (Peacock and Sanderson, 1991). The rapid change in displacement across the link for straight segments may relate to the fact that, during the continued history of slip accumulation, the combined system absorbs more strain, whereas the straight tip is isolated and passive.

Many of the hard-linked systems in the study area contain multiple links with internally consistent geometries along strike, as shown in Fig. 2(c). The relative age model indicated by Cruikshank and Aydin (1995) implies that the system propagated in one direction, whereas the local propagation direction may be reversed along individual segments (Fig. 12). If this model is correct, segment 1 (in Fig. 12) existed as an isolated structure before segment 2 grew towards, and linked with, segment 1. Similarly, the opposite tip of segment 2 was isolated before being approached by segment 3, and so on. This indicates that systems like 96-19 in Fig. 9 may, on the scale of the entire system, have grown from one end to the other rather than from its final centre.

A second type of connected or hard-linked systems of deformation band segments is known as horse-tailing systems, where single deformation bands splay into a series of approximately straight segments that eventually die out (Fig. 7f). Three examples of horse-tail terminations have been examined, of which two (96-8 and 96-9 in Fig. 9) show a higher displacement gradient than the opposite part of the systems, and one (96-7 in Fig. 8) exhibits a more gentle displacement gradient.

Other types of hard links include the case where two approaching segments curve and join at two points to form a hard-linked eye-structure of the type shown in Figs 3(c) & 7(e). It was not possible to examine these structures in any detail because of their small scale.

During the development of hard-linked systems, a plateau-type displacement profile is generated that may be preceded by a single peak profile if growth pursues without further linkage. Prior to the plateau stage, an intermittent stage of multipeak displacement profile is expected, as seen in Fig. 9 (96-3). The schematic development of a displacement profile along a hard-linked system is similar to that of a soft-linked system, and Fig. 10 thus applies to both. The only difference between the two, both having an early history as soft-linked systems, is that strain is transferred ductilely

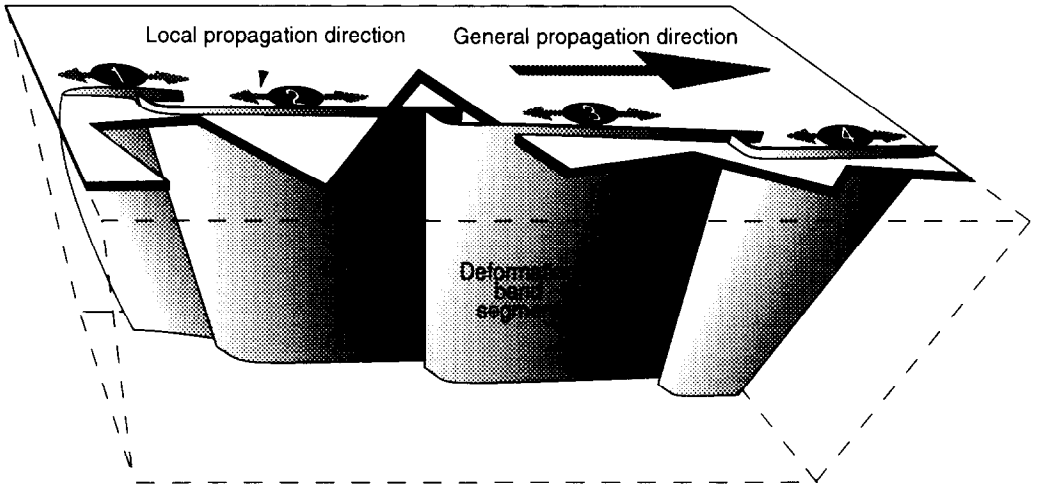

Fig. 12. Geometric appearance of several hard-linked systems of deformation bands. If the assumption that the curving tail is younger than the interconnected straight tip of the neighbouring segment, the local propagation direction is locally opposite to that of the system as a whole, which indicates that the system mainly grew from one end towards the other.

rather than brittlely across the linked regions in soft-linked systems. Indeed, hard-linked structures may change to become soft links in the vertical dimension, and the distinction is thus confined to the horizontal section studied.

Deformation band cluster zones

The linked systems discussed above are simple, but much more complex systems occur in the field area. Systems of deformation bands connected through hard or soft links form complex zones of deformation bands (cluster zones) (Fig. 3b). Zones that are about 10 cm wide or more typically have an associated polished slip surface, and extend laterally for several hundreds of metres. Unfortunately, the exposures are not continuous enough in the area to measure the length/displacement ratio of these zones.

The developmental model for faults in porous sandstones in southeastern Utah put forward by Aydin and Johnson (1978, 1983) also applies to the present study area. Three sequential stages are defined: (1) formation of *ca* 1 mm thick deformation bands; (2) zones of deformation bands consisting of numerous closely spaced deformation bands with aggregate offsets of a few, or tens of, centimetres; and (3) slip surfaces in zones of deformation bands. We interpret the linked systems described above to represent the intermediate stages between (1) and (2).

The thickness of the deformation zone increases during this development, but individual deformation bands in the zones have the same thickness as single, isolated, ones. This is because the deformation zone grows by continual formation of new deformation bands rather than by widening of old ones (Fig. 3b). The mechanical cause for this strain-hardening process is described in detail by Aydin (1978) and Aydin and Johnson (1978) as collapse of pore space by compaction, consolidation and subsequent cataclastic processes.

The mechanically polished slip surfaces contain abundant striations indicating dip-slip movements (Fig. 1, inset). Corrugation structures that are best exposed along the margins of the deformation band cluster zones (Fig. 3d) show identical (i.e. slip-parallel) orientations. These corrugations are curved segments of deformation bands that are completely linked with other curved deformation bands. The width of each corrugation structure is about 2–10 cm, whereas they are commonly 1 m long or more in the slip direction. A section through the cluster zones (e.g. Fig. 3b) reveals a curving, anastomosing network of deformation bands. A line profile through such a cluster zone would typically intersect a few tens of deformation bands.

Gentle undulations occur that are second-order to (about one order of magnitude larger than) the corrugations mentioned above. Also, these linear structures appear to be parallel to the slip direction of the fault.

Scaling relations

The scaling relation between length and maximum displacement of the isolated deformation bands has been analysed statistically and by plotting the population in a log–log plot as shown in Fig. 13. In the log–log plot, the data fit well to a straight line with a slope of 0.54 (simple t-statistics show that, at the 5% significance level, there is a significant linear correlation for the dataset; see Appendix). In other words, if the relationship between maximum displacement (D_{max}) and length (L) of the deformation bands is expressed as

$$D_{max} = cL^b \quad (1)$$

where c is a constant, then $b = 0.54$ and $c = 0.0016$ in the present case. This means that long deformation bands have relatively larger maximum displacements than short bands. It can be seen from Fig. 5 that peak-type profiles have higher D_{max}/L ratios than plateau-type profiles,

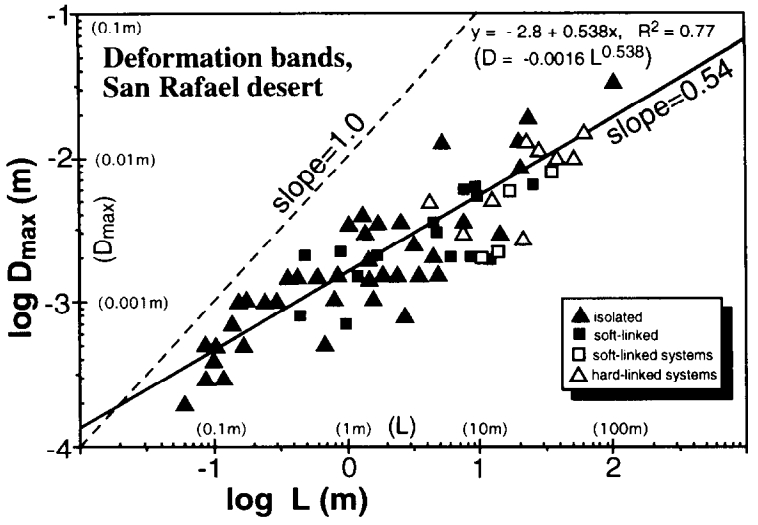

Fig. 13. Length (L) vs maximum displacement (D_{max}) for the deformation bands studied in this work, plotted in log–log space. A well-defined curve with a slope (exponent) of 0.54 is fitted to the data from isolated deformation bands. Individual soft-linked segments and full soft- and hard-linked systems also fit this curve quite well. The hard-linked system alone has a slope of 0.49. A line with slope of 1 is shown for comparison.

which to some extent is reflected by the scatter of points in Fig. 13.

Individual segments of soft-linked systems are also plotted in Fig. 13, as are the total length and corresponding maximum displacement of both soft- and hard-linked systems (see Appendix for a statistical analysis). As expected, the latter two datasets mostly plot below the line with $b = 0.54$ (line fitted to the isolated deformation bands). The reason for this is that linkage immediately leads to increased length, while displacement accumulates gradually (Fig. 10) (see also Cartwright *et al.*, 1995). Nevertheless, the linked systems plot within the range of variation observed among the isolated deformation bands, and the slope (power-law exponent b) for all data shown in Fig. 13 is 0.49. The few soft-linked systems do not show a significant linear correlation at the 95% confidence level. However, a significant linear correlation exists for the hard-linked systems, and the slope (b) is calculated to be 0.49. There is no significant difference between this slope and the slope of 0.54 for isolated deformation bands.

Size (displacement or length) distributions of isolated deformation bands from the surface studied (Fig. 1) are presented as cumulative number plots in Fig. 14. Both length and maximum displacement values lie along curves that have straight central segments, typical of most published cumulative frequency plots (e.g. Pickering *et al.*, 1995). This indicates a power-law distribution of fault sizes of the form:

$$N = aL^{-S} \tag{2}$$

or

$$N = aD_{max}^{-S}, \tag{3}$$

where N is the cumulative number, a is a constant, L is length, D_{max} is the maximum displacement and the exponent S reflects the slope of the straight curve segment. Undersampling of the smaller deformation bands can be used to explain the break in slope at about $D_{max} = 1$ mm in Fig. 14(a), and at $L = 1$ m in Fig. 14(b) (cf. Pickering *et al.*, 1995). The exponent for the displacement population (0.9) falls in the low end of the general range of previously reported data (the common range is 1.0–1.5), whereas an exponent of 0.6 for the length population is significantly lower than those commonly reported for larger faults or faults with well-developed slip surfaces (e.g. Yielding *et al.*, 1996; see also Cladouhos and Marrett, 1996). However, faults in the Jurassic Navajo Sandstone in Chimney rock, San Rafael Swell, Utah, are different and show a slope of 0.67 (Krantz, 1988; Cladouhos and Marrett, 1996, fig. 1). This value is close to that of this study, and occurs in nearby rocks of similar lithology (porous sandstones) and age.

DISCUSSION

Many of the geometrical aspects of deformation bands presented in this work are similar to those reported for other faults (faults with discrete slip surfaces). Both show characteristic displacement profiles with increasing displacement towards a maximum value near the middle of the structure. As shown in Fig. 11, the displacement maximum is offset from the centre towards the overlapping tip for soft-linked systems. This feature is also reported from larger fault systems (e.g. Peacock and Sanderson, 1991; Dawers *et al.*, 1993; Childs *et al.*, 1995; Dawers and Anders, 1995), and has been modelled numerically using a three-dimensional boundary element program by Willemse *et al.* (1996). The fact that some apparently isolated deformation bands show asymmetric displacement profiles may be explained by variations in

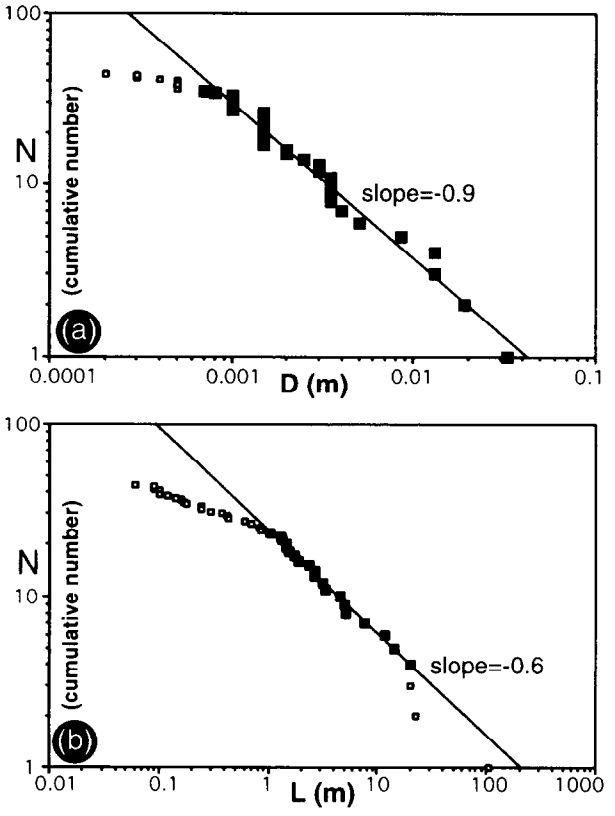

Fig. 14. (a) Maximum displacement of isolated deformation bands plotted against cumulative number (N). (b) Length of isolated deformation bands plotted against cumulative number (N). See text for discussion.

propagation rate due to intersection with other structures above or below the exposed horizontal section, non-planar fault surfaces (fault bends) and lithological contrasts (e.g. Peacock and Sanderson, 1996).

It has been suggested (Childs *et al.*, 1995; Dawers and Anders, 1995) that isolated faults may grow and link to form a system where the total displacement profile resembles that of an isolated fault of the same length (i.e. a geometrically coherent system). This evolution is reflected in the data presented above, where various stages in the linking process of deformation bands are recognized (Fig. 10).

Differences between faults and deformation bands

In spite of the abovementioned similarities between deformation bands and faults in general, the difference in the displacement–length relationship requires further attention. For faults with lengths in excess of *ca* 100 m, a power-law relationship between length and displacement (equation (1)) is generally accepted in the literature. However, the value of the exponent has been the matter of some debate. Workers who have analysed compiled datasets have suggested that the exponent (n) is 2 (Walsh and Watterson, 1988) or 1.5 (Marrett and Allmendinger, 1991; Walsh and Watterson, 1991). Others, who have studied individual datasets, indicate that $n \approx 1$ for small faults (Muraoka and Kamata, 1983; Schlische *et al.*, 1996) as well as for larger faults (Elliott, 1976; Opheim and Gudmundsson, 1989; Gudmundsson, 1992; Dawers *et al.*, 1993; Carter and Winter, 1995; Villemin *et al.*, 1995; also see discussions by Cowie and Scholz, 1992). Clark and Cox (1996) point out the importance of statistical analysis of the displacement–length data and, after reconsideration of most of the existing datasets, conclude that an exponent of 1 (linear relationship) explains most of the sets. In contrast to these findings, the present dataset from a population of deformation bands indicates an exponent which is closer to 0.5, and is thus different from the majority of previously published fault datasets (Fig. 15).

We suggest that growth of deformation band populations with cataclasis in the Entrada Sandstone follows a D_{max}–L scaling law with an exponent of ≈ 0.5 only until a slip surface forms, i.e. after the formation of *ca* 10 cm wide cluster zones with aggregate displacement on the order of a few tens of centimetres (Fig. 15). The population of slip surfaces themselves are expected to grow like any other fault population and thus may follow a linear exponent. Restricted exposure prevented us from collecting sufficient D–L data from faults with striated slip surfaces in the Goblin Valley area to demonstrate this change in scaling law directly. However, data from such faults are available from the well-exposed and nearby Chimney rock area of the northern part of San Rafael Swell (Krantz, 1988). Here, faults with well-developed slip surfaces occur in porous sandstones of the Navajo Sandstone and lower Carmel Formation, which closely resemble those of the overlying Entrada Formation in the

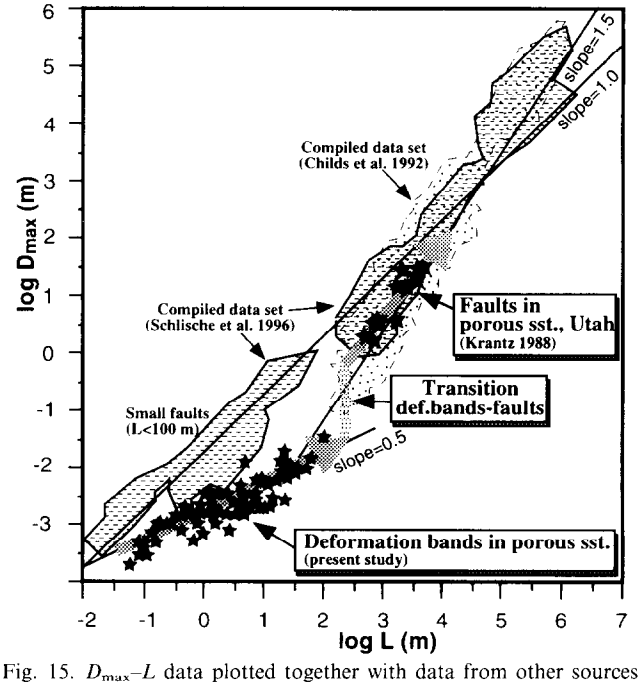

Fig. 15. D_{max}–L data plotted together with data from other sources (cited in Schlische *et al.*, 1996 and Gillespie *et al.*, 1992). See text for discussion.

Goblin Valley area. As can be seen from Fig. 15, the fault data reported by Krantz (1988) fall within the field of D_{max}–L data reported for other faults of similar size, and appear to conform to a scaling exponent between 1.0 and 1.5. This finding implies that fault displacement–length relationships should not be scaled down to the size of deformation bands in a porous sandstone if deformation bands are present.

We believe that the special D_{max}–L scaling relationship discovered for deformation bands, and thus the related fault-growth model, is somehow related to the fundamental differences between deformation bands and other types of faults. Existing models of fault growth are based on simple models where faults are (planar) discontinuities or cracks in otherwise elastic or elastic–plastic material (Cowie and Scholz, 1992). These conditions fail for deformation bands, which in the study area show clear evidence of profound strain hardening without development of weak (soft) slip surfaces until they reach an advanced stage (Aydin and Johnson, 1978, 1983). Strain hardening causes widening of the deformation band and continual formation of new deformation bands, resulting in populations of isolated deformation bands, linked deformation bands and/or deformation band cluster zones. This entire development occurs without development of discontinous surfaces or cracks, and is therefore fundamentally different to faults with well-developed slip surfaces where displacement very much accumulates repeatedly on the slip surface to produce much larger finite displacement.

The exact scaling law exponent (≈ 0.5) calculated for the San Rafael Desert dataset is not necessarily generally applicable to porous sandstones. As mechanical and lithological differences may control the scaling relationships, similar studies of deformation bands in sandstones with other physical properties are necessary when approaching this question.

Application to the petroleum industry

Small-scale (subseismic) faults or deformation bands may have an important influence on reservoir performance as they may represent significant barriers to fluid flow during oil production (e.g. Antonellini and Aydin, 1994). Their nature and spatial distribution can in each case be approached by the use of attribute maps and core data (e.g. Hesthammer and Fossen, 1997). Our work in Utah indicates that seismically resolvable faults cannot be scaled down to the size range of deformation bands, although this assumption is sometimes applied as input to reservoir simulation models (e.g. Gauthier and Lake, 1993). Along with parameters such as orientation, distribution and frequency, the length of the deformation band is of primary importance in the oil industry, particularly because long bands are more likely to interconnect than shorter ones. Down-scaling of the established D_{max}–L relationship for published fault populations (excluding deformation bands) roughly indicates that a fault with a maximum displacement of 2 cm has a length of the order of 1 m (line with slope = 1.0 in Fig. 15). However, a deformation band with an identical displacement in a porous sandstone should be about 100 m long according to the data presented above (Fig. 13). This profound difference in length may indeed have dramatic effects on models of reservoir performance, and deformation bands with apparent offset of the order of a few centimetres should not be neglected unless it can be demonstrated that they do not act as significant barriers to fluid flow during production.

CONCLUSIONS

Deformation bands in the San Rafael Desert, Utah, U.S.A., show many similarities with other types of faults of similar and larger size, including upward-convex displacement profiles and soft- and hard-linked geometries with a steeper displacement gradient near the link or overlap zone. The deformation bands are, however, ruled by strain-hardening processes, which cause the formation of deformation band cluster zones and eventually to the formation of a through-going, weak slip surface that accommodates most subsequent strain. Prior to this stage, deformation bands in the study area do not follow the linear scaling relationship between displacement and length recorded in many fault populations, but obey a power-law relationship with an exponent close to 0.5. We are not able to provide a sound explanation for this observation, which may imply a separate fault-growth law for deformation bands in porous sandstones. However, the exponent is well defined, partly because the dataset spans more than three orders of magnitude with respect to fault length. It is not known whether this exponent is common to all porous sandstones, but it is expected to be similar for deformation band populations in porous sandstones where the deformation bands involve cataclastic processes. The presence of a change in exponent of the displacement–length relationship has important consequences for strain determinations and the down-scaling of larger faults, which again is of importance in evaluation or simulation of fluid flow in a reservoir rock. Additional studies of the same type are crucial to determine the generality of this discovery.

Acknowledgements—We are grateful to Statoil for financial support, to R. H. Gabrielsen, N. Odling and W. Nemec for commenting on an earlier version of the manuscript, and for helpful referee comments by N. Dawers and K. E. Carter Krogh.

REFERENCES

Antonellini, M. and Aydin, A. (1994) Effect of faulting on fluid flow in porous sandstones: petrophysical properties. *Bulletin of the American Association of Petroleum Geologists* **78**, 355–377.

Antonellini, M. and Aydin, A. (1995) Effect of faulting on fluid flow in porous sandstones: geometry and spatial distribution. *Bulletin of the American Association of Petroleum Geologists* **79**, 642–671.

Antonellini, M. A., Aydin, A. and Pollard, D. D. (1994) Microstructure of deformation bands in porous sandstones at Arches National Park, Utah. *Journal of Structural Geology* **16**, 941–959.

Aydin, A. (1978) Small faults formed as deformation bands in sandstone. *Pure and Applied Geophysics* **116**, 913–930.

Aydin, A. and Johnson, A. M. (1978) Development of faults as zones of deformation bands and as slip surfaces in sandstones. *Pure and Applied Geophysics* **116**, 931–942.

Aydin, A. and Johnson, A. M. (1983) Analysis of faulting in porous sandstones. *Journal of Structural Geology* **5**, 19–31.

Aydin, A. and Reches, Z. (1982) The number and orientation of fault sets in the field and in experiments. *Geology* **10**, 107–112.

Baker, A. A. (1946) Geology of the Green River Desert—Cataract Canyon region, Emery, Wayne and Garfield Counties, Utah. *U.S. Geological Survey Bulletin* **951**.

Carter, K. E. and Winter, C. L. (1995) Fractal nature and scaling of normal faults in the Espanola Basin, Rio Grande rift, New Mexico: implications for fault growth and brittle strain. *Journal of Structural Geology* **17**, 863–873.

Cartwright, J. A., Trudgill, B. D. and Mansfield, C. S. (1995) Fault growth by segment linkage: an explanation for scatter in maximum displacement and trace length data from the Canyonlands Grabens of SE Utah. *Journal of Structural Geology* **17**, 1319–1326.

Childs, C., Watterson, J. and Walsh, J. J. (1995) Fault overlap zones within developing normal fault systems. *Journal of the Geological Society of London* **152**, 535–549.

Cladouhos, T. T. and Marrett, R. (1996) Are fault growth and linkage models consistent with power-law distributions of fault lengths? *Journal of Structural Geology* **18**, 281–293.

Clark, R. M. and Cox, S. J. D. (1996) A modern regression approach to determining fault displacement scaling relationships. *Journal of Structural Geology* **18**, 147–152.

Cowie, P. A. and Scholz, C. H. (1992) Displacement–length scaling relationship of faults using a post-yield fracture mechanics model. *Journal of Structural Geology* **14**, 1133–1148.

Cruikshank, K. M. and Aydin, A. (1995) Unweaving the joints in Entrada Sandstone, Arches National Park, Utah, U.S.A *Journal of Structural Geology* **17**, 409–421.

Cruikshank, K. M., Zhao, G. and Johnson, A. M. (1991) Analysis of minor fractures associated with joints and faulted joints. *Journal of Structural Geology* **13**, 865–886.

Dawers, N. H. and Anders, M. H. (1995) Displacement-length scaling and fault linkage. *Journal of Structural Geology* **17**, 607–614.

Dawers, N. H., Anders, M. H. and Scholz, C. H. (1993) Growth of normal faults: Displacement–length scaling. *Geology* **21**, 1107–1110.

Elliott, D. (1976) The energy balance and deformation mechanisms of thrust sheets. *Philosophical Transactions of the Royal Society of London* **A283**, 289–312.

Fowles, J. and Burley, S. (1994) Textural and permeability characteristics of faulted, high porosity sandstones. *Marine and Petroleum Geology* **11**, 608–623.

Gabrielsen, R. H. and Koestler, A. G. (1987) Description and structural implications of fractures in late Jurassic sandstones of the Troll Field, northern North Sea. *Norsk Geologisk Tidsskrift* **67**, 371–381.

Gauthier, B. D. M. and Lake, S. D. (1993) Probabilistic modeling of faults below the limit of seismic resolution in Pelican Field, North Sea, offshore United Kingdom. *Bulletin of the American Association of Petroleum Geologists* **77**, 761–777.

Gillespie, P. A., Walsh, J. J. and Watterson, J. (1992) Limitations of dimension and displacement data from single faults and the consequences for data analysis and interpretation. *Journal of Structural Geology* **14**, 1157–1172.

Gudmundsson, A. (1992) Formation and growth of normal faults at the divergent plate boundary in Iceland. *Terra Nova* **4**, 464–471.

Hesthammer, J. and Fossen, H. (1997) Seismic attribute mapping for structural interpretation of the Gullfaks Field, northern North Sea. *Petroleum Geoscience* **3**, 13–26.

Horsfield, W. T. (1980) Contemporaneous movement along crossing conjugate normal faults. *Journal of Structural Geology* **2**, 305–310.

Huggins, P., Watterson, J., Walsh, J. J. and Childs, C. (1995) Relay zone geometry and displacement transfer between normal faults recorded in coal-mine plans. *Journal of Structural Geology* **17**, 1741–1755.

Jamison, W. R. (1982) Tectonic deformation of Wingate Sandstone, Colorado National Monument. *Bulletin of the American Association of Petroleum Geologists* **66**, 2584–2608.

Krantz, R. W. (1988) Multiple fault sets and three-dimensional strain: theory and application. *Journal of Structural Geology* **10**, 225–237.

Marrett, R. and Allmendinger, R. W. (1990) Kinematic analysis of fault-slip data. *Journal of Structural Geology* **12**, 973–986.

Marrett, R. and Allmendinger, R. W. (1991) Estimates of strain due to brittle faulting: sampling fault populations. *Journal of Structural Geology* **13**, 735–738.

Muraoka, H. and Kamata, H. (1983) Displacement distribution along minor fault traces. *Journal of Structural Geology* **5**, 483–495.

Nicol, A., Watterson, J., Walsh, J. J. and Childs, C. (1996) The shapes, major axis prientations and displacement patterns of fault surfaces. *Journal of Structural Geology* **18**, 235–248.

Olson, J. and Pollard, D. D. (1989) Inferring paleostresses from natural fracture patterns: a new method. *Geology* **17**, 345–348.

Opheim, J. A. and Gudmundsson, A. (1989) Formation and geometry of fractures, and related volcanism, of the Krafla fissure swarm, northeast Iceland. *Bulletin of the Geological Society of America* **101**, 1608–1622.

Peacock, D. C. P. and Sanderson, D. J. (1991) Displacements, segment linkage and relay ramps in normal fault zones. *Journal of Structural Geology* **13**, 721–733.

Peacock, D. C. P. and Sanderson, D. J. (1994) Geometry and development of relay ramps in normal fault systems. *Bulletin of the American Association of Petroleum Geologists* **78**, 147–165.

Peacock, D. C. P. and Sanderson, D. J. (1996) Effects of propagation rate on displacement variations along faults. *Journal of Structural Geology* **18**, 311–320.

Pickering, G., Bull, J. M. and Sanderson, D. J. (1995) Sampling power-law distributions. *Tectonophysics* **248**, 1–20.

Pittman, E. D. (1981) Effect of fault-related granulation on porosity and permeability of quartz sandstones, Simpson Group (Ordovician), Oklahoma. *Bulletin of the American Association of Petroleum Geologists* **65**, 2381–2387.

Pollard, D. D. and Segall, P. (1987) Theoretical displacements and stresses near fractures in rock: with applications to faults, joints, veins, dikes, and solution surfaces. In *Fracture Mechanics of Rock*, ed. B. Atkinson, pp. 277–349. Academic Press, London.

Ramsay, J. G. (1980) Shear zone geometry: a review. *Journal of Structural Geology* **2**, 83–99.

Rigby, J. K. (1987) *Stratigraphy and Structure of the San Rafael Reef, Utah; A Major Monocline of the Colorado Plateau*, pp. 269–273. Geological Society of America Centennial Field Guide—Rocky Mountains Section.

Schlische, R. W., Young, S. S., Ackermann, R. V. and Gupta, A. (1996) Geometry and scaling relations of a population of very small rift-related normal faults. *Geology* **24**, 683–686.

Scholz, C. H., Dawers, N. H., Yu, J. Z. and Anders, M. H. (1993) Fault growth and fault scaling laws: preliminary results. *Journal of Geophysical Research* **98**, 21951–21961.

Trudgill, B. and Cartwright, J. (1994) Relay-ramp forms and normal-fault linkages, Canyonland National Park, Utah. *Bulletin of the Geological Society of America* **106**, 1143–1157.

Underhill, J. R. and Woodcock, N. H. (1987) Faulting mechanisms in high-porosity sandstones: New Red Sandstone, Arran, Scotland. In *Deformation of Sediments and Sedimentary Rocks*, eds M. E. Jones and R. M. F. Preston, pp. 91–105. Geological Society of London Special Publication **29**.

Villemin, T., Angelier, J. and Sunwoo, C. (1995) Fractal distribution of fault length and offsets: implications of brittle deformation evaluation—Lorraine Coal Basin. In *Fractals in the Earth Sciences*, eds C. C. Barton and P. R. LaPointe, pp. 205–226. Plenum Press, New York.

Walsh, J. J. and Watterson, J. (1988) Analysis of the relationship between displacements and dimensions of faults. *Journal of Structural Geology* **10**, 239–247.

Walsh, J. J. and Watterson, J. (1991) Geometric and kinematic coherence and scale effects in normal fault systems. In *The Geometry of Normal Faults*, eds A. M. Roberts, G. Yielding and B. Freeman, pp. 193–203. Geological Society of London Special Publication **56**.

Willemse, E. J. M., Pollard, D. D. and Aydin, A. (1996) Three-dimensional analyses of slip distributions on normal fault arrays with consequences for fault scaling. *Journal of Structural Geology* **18**, 295–309.

Yielding, G., Needham, T. and Jones, H. (1996) Sampling of fault populations using sub-surface data: a review. *Journal of Structural Geology* **18**, 135–146.

APPENDIX

The measurements of maximum displacement and length of deformation bands are divided into the following datasets: (1) isolated deformation bands; (2) deformation band segments in soft-linked systems; (3) soft-linked systems (the entire system treated as a single structure); (4) hard-linked systems (the entire system treated as a single structure); and (5) the total dataset ((1)–(4) combined). We assume that the accuracy of the length measurements is more precise than the measurements of displacement, which justifies an application of the standard method of least-squares regression to the datasets (Clark and Cox, 1996). The goodness-of-fit of the regression lines calculated for the datasets is high ($R^2 > 0.7$) except for set (3) ($R^2 = 0.53$) and set (4) ($R^2 = 0.46$), which is probably related to the limited size and ranges of sets (3) and (4). The correlation coefficient (R) indicates the fit of the data to a single line, but says nothing about the slope of that line or whether a significant linear correlation exists (Clark and Cox, 1996). To test the significance of the linear correlations, Fisher's t-test was applied to the individual datasets, under the assumption that the data derive from populations with normal distributions.

The test is used here in its convenient 'one-tail' version, with the null hypothesis stating that the calculated correlation values are not significantly higher than zero. An analogous one-tail test has further been applied to test the significance of the linear regressions, with the null hypothesis that the regression line's gradient is not significantly different from zero. The results of both tests are summarized in Table 1. The null hypothesis has been rejected at a confidence level of 95% in all instances, except for the soft-linked systems where the null hypothesis could not be rejected with a confidence of at least 95% ($\alpha = 5\%$).

The datasets representing all deformation bands (combined data) and the isolated deformation bands have further been tested for the difference between their individual regressions, using the Fisher 'line-parallelism' test. The results are given in Table 2. The 'one-tail' null hypothesis here states that the latter regression (estimated as $b = 0.49$) is not significantly smaller than the former regression (estimated as $b = 0.54$). The test suggests that the two regression lines are parallel at a confidence level higher than 95% ($\alpha = 5\%$). A similar result has been obtained from the test of the regression lines between the isolated deformation bands and the hard-linked systems (Table 2).

Table 1. Results of Fisher's t-tests of the significance of the linear correlations and regressions

Set	N	R	t_{calc}	$t_{\alpha=5\%}$	c	b	t_{calc}	$t_{\alpha=5\%}$
Isolated deformation bands	44	0.88	11.7	1.68	−2.80	0.54	4.01	1.68
Deformation band segments within soft-linked systems	16	0.73	3.96	1.76	−2.83	0.40	23.66	1.76
Soft-linked systems	4	0.88	2.66	2.92	−3.87	1.18	73.40	2.92
Hard-linked systems	9	0.68	2.47	1.90	−2.79	0.49	36.25	1.90
All deformation bands (combined)	73	0.87	14.88	1.67	−2.83	0.49	112.1	1.67

N, number of data points; R, the coefficient of linear correlation; c, the regression line's point of intersection with the independent variable's axis; b, the regression line's gradient (slope); t_{calc}, calculated test statistics; $t_{\alpha=5\%}$, critical value for selected α; α, significance level (%).

Table 2. The results of Fisher's t-tests of regression line parallelism for three selected datasets

Type	N	S^2	ΣZ^2	c	b	t_{calc}	$t_{\alpha=5\%}$
Isolated deformation bands	44	0.24	10.2	−2.80	0.54	–	–
All deformation bands (combined)	73	0.22	15.7	−2.83	0.49	–	–
Hard-linked systems	9	0.09	0.62	−2.79	0.49	–	–
Fisher's t-test for the isolated deformation bands and the combined dataset						0.24	1.66
Fisher's t-test for the isolated bands and hard-linked systems					—	0.09	1.68

N, number of data; S^2, the variance of the residual component; ΣZ^2 is the sum of squared residuals; c, b, t_{calc}, $t_{\alpha=5\%}$ and α are as in Table 1.